Type of manuscript: Article

Supporting Information

Simulation-guided synthesis of graphitic carbon nitride beads with 3D interconnected and continuous meso/macropore channels for enhanced light absorption and photo-catalytic performance

Yudong Li,[a,1] Yanqiu Jiang,[a,1] Zhaohui Ruan,[b] Kaifeng Lin,*[a] Zhuobin Yu,[c] Zhanfeng Zheng,[c] Xianzhu Xu,[a] and Yuan Yuan,*[b]

[a]MIIT Key Laboratory of Critical Materials Technology for New Energy Conversion and Storage, School of Chemistry and Chemical Engineering, Harbin Institute of Technology, Harbin 150001, China. *Emails of corresponding authors: linkaifeng@hit.edu.cn

[b]School of Energy Science and Engineering, Harbin Institute of Technology, Harbin 150001, China. *Emails of corresponding authors: yuanyuan83@hit.edu.cn

[c]State Key Laboratory of Coal Conversion, Institute of Coal Chemistry, Chinese Academy of Sciences, Taiyuan 030001, China

[1] Y. Li and Y. Jiang contributed equally to this work.

Supporting Figures (S1-S23), Tables (S1-S6).

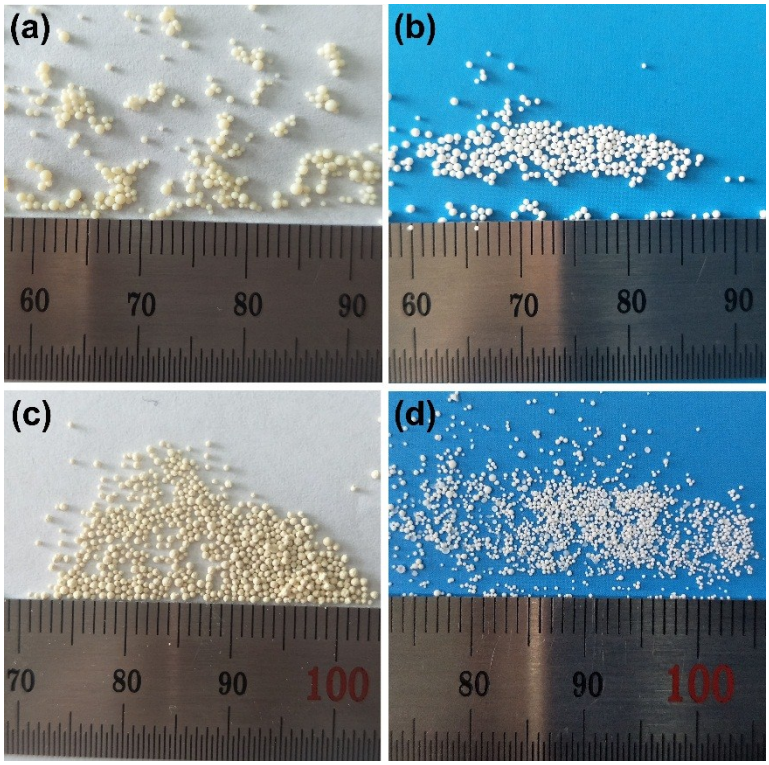

Figure S1 Morphology of (a) IRA-900 beads, (b) porous silica beads, (c) MCN-560 beads and (d) reversed porous silica beads.

Table S1 Parameter setting in FDTD simulation.

Diamete	Meshing parameter			Boundary condition		
r	Δx	Δy	Δz	x	y	z
5	0.1	0.1	1	periodic	periodic	PML
10	0.5	0.5	1	periodic	periodic	PML
50	0.5	0.5	1	periodic	periodic	PML
80	1	1	1	periodic	periodic	PML

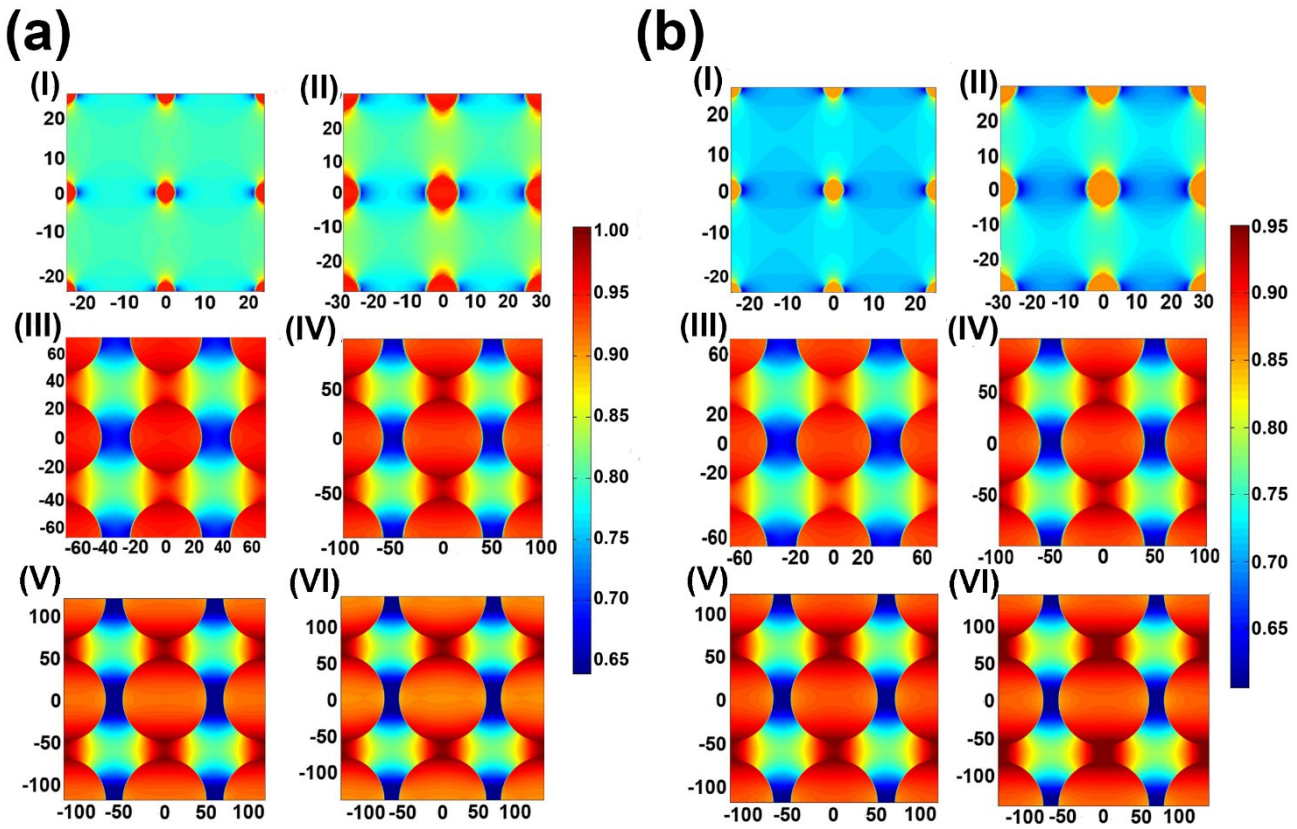

Figure S2 Distribution of electrical field at the section of (a) 50 nm from the entrance of the pore channel and (b) 90 nm from the entrance of the pore channel, Panels marked (I), (II), (III), (IV), (V) and (VI) correspond to the pore sizes of d = 5, 10, 50, 80, 100 and 120 nm respectively. All the units are nm.

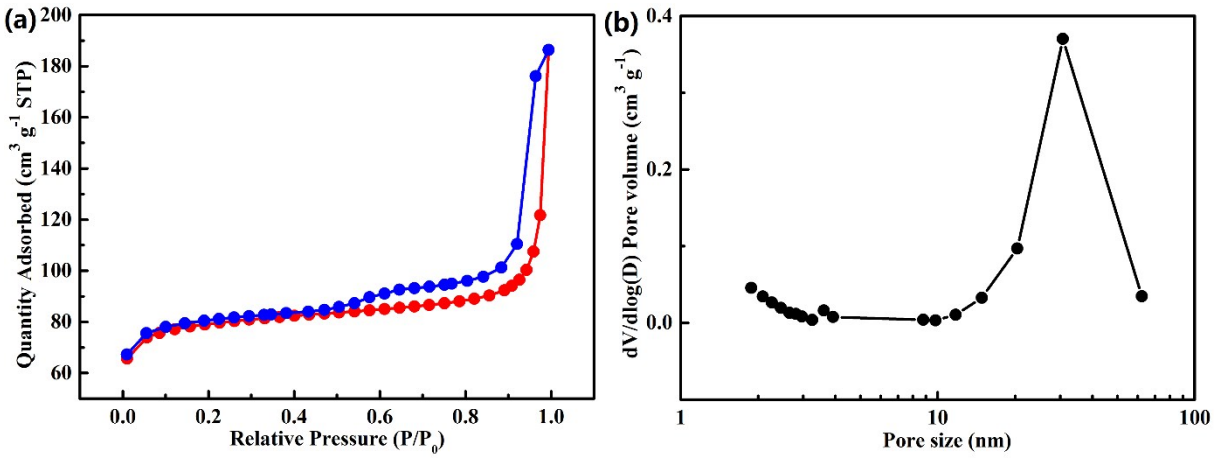

Figure S3 (a) Nitrogen adsorption-desorption isotherms and (b) the corresponding pore size distribution curves of silica beads.

Table S2 S_{BET} and pore volume of SiO_2 beads and MCN materials.

Materials	S_{BET} [m^2 g^{-1}]	Pore Volume [cm^3 g^{-1}]
SiO_2 beads	304	0.14
MCN-530	49	0.14
MCN-550	52	0.13
MCN-560	58	0.15
MCN-570	51	0.15
MCN-580	49	0.14

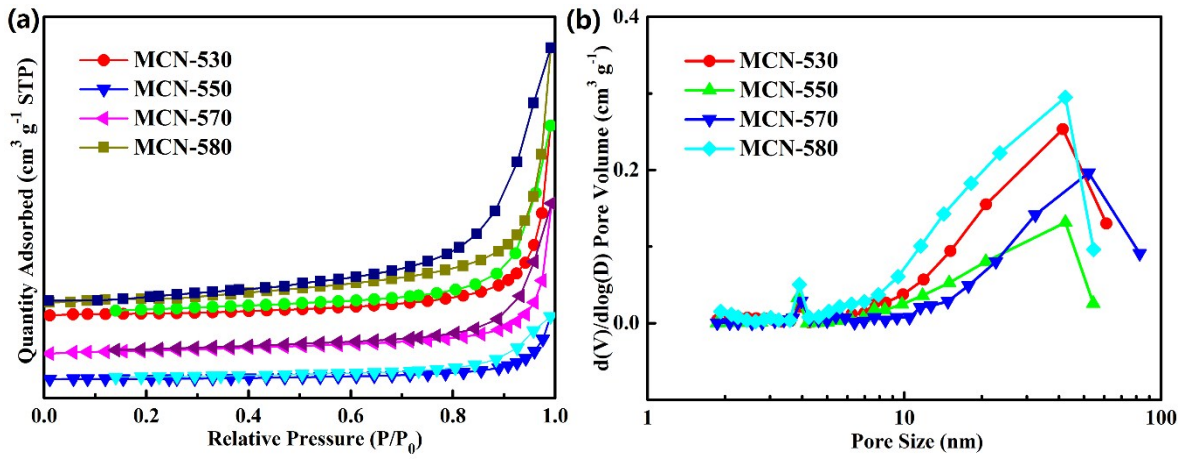

Figure S4 (a) Nitrogen adsorption-desorption isotherms and (b) the corresponding pore size distribution curves of MCN-530, MCN-550, MCN-570 and MCN-580.

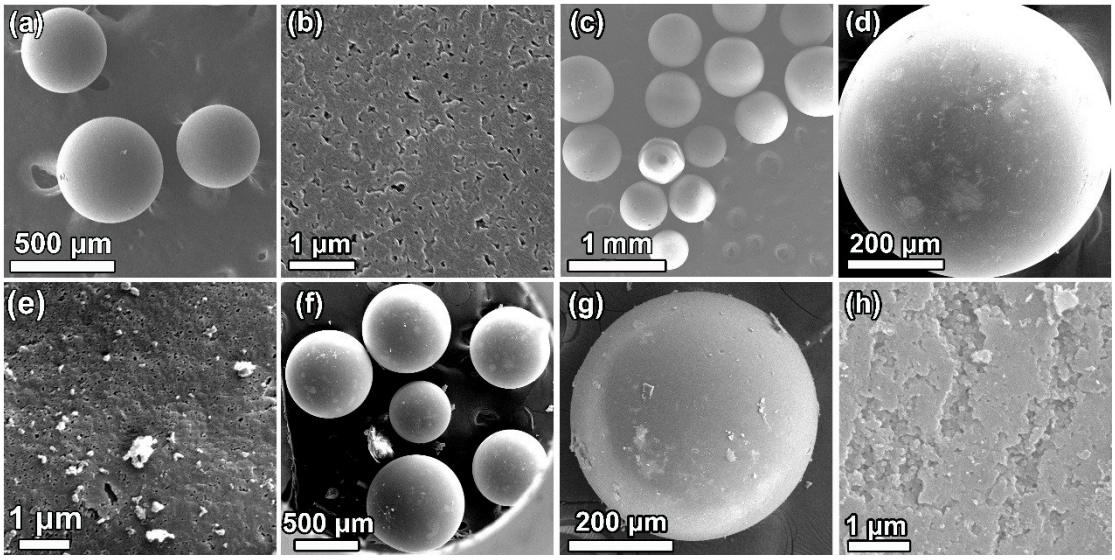

Figure S5 SEM images of (a) IRA-900 bead, (b) surface of IRA-900, (c, d) SiO_2 beads, (e) surface of SiO_2 bead, (f, g) reverse SiO_2 beads with MCN-560 as templates, (h) surface of reverse SiO_2 beads with MCN-560 as templates.

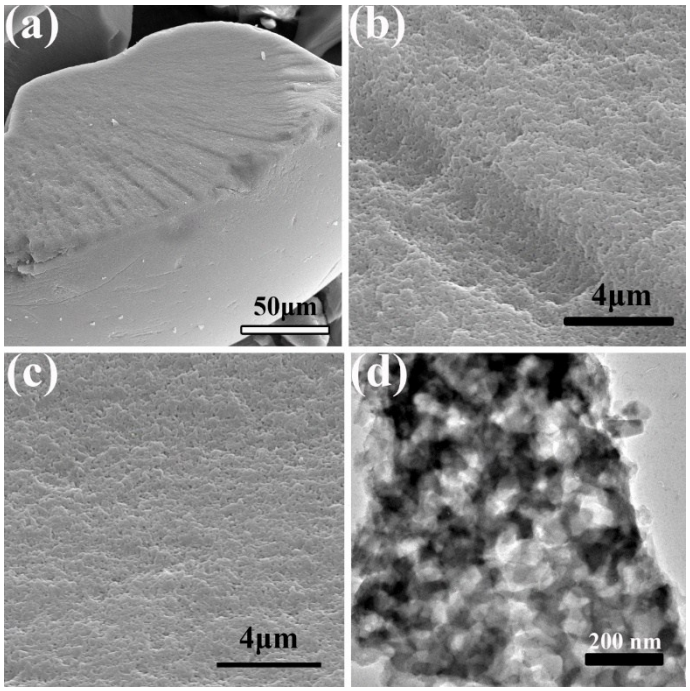

Figure S6 (a, b and c) SEM images and (d) TEM images of inner structure of silica bead.

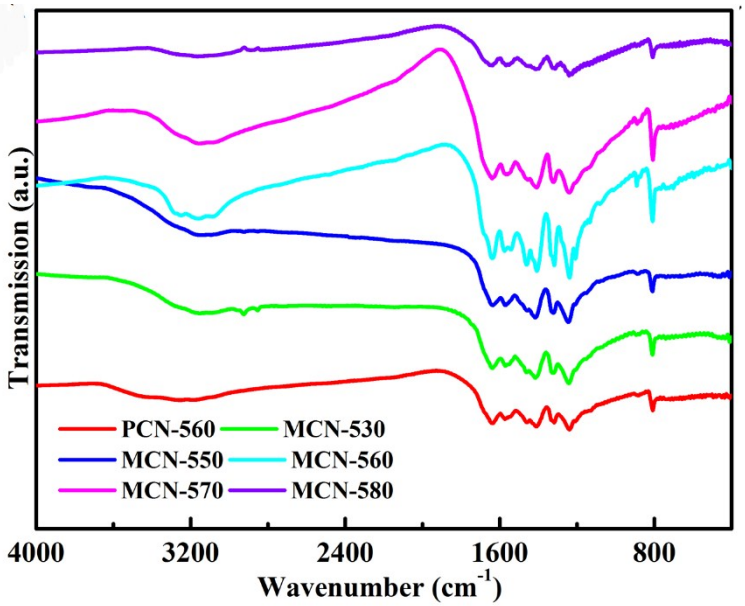

Figure S7 FT-IR spectra of PCN-560 and MCN materials in different sintering temperatures.

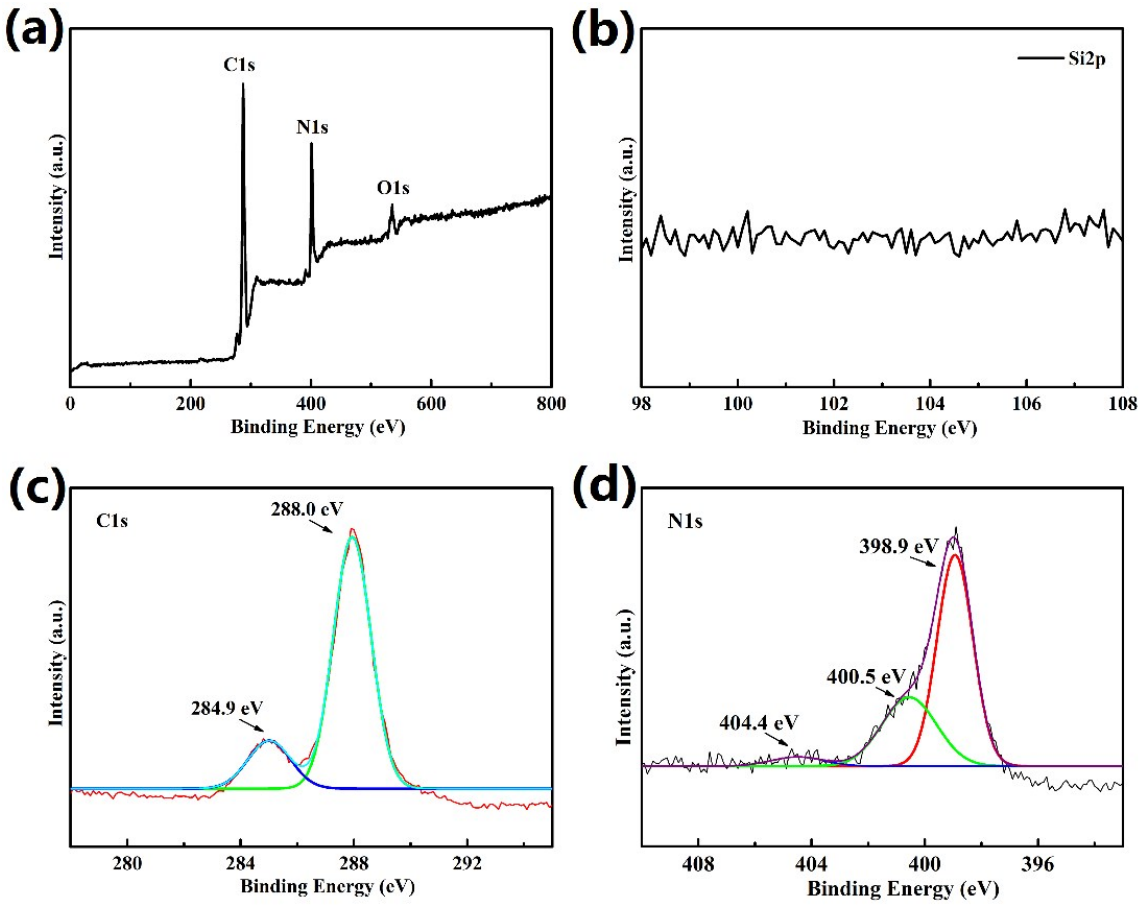

Figure S8 XPS spectra: (a) total spectra, (b) Si2p spectra, (c) C1s spectra and (d) N1s spectra of MCN-560.

Table S3 Elemental composition of $C_2N_4H_4$ precursor, PCN and MCN materials obtained from CHN analysis.

Materials	Content [wt %]				C/N Ratio [in mole]
	C	N	O	H	
$C_2N_4H_4$	28.5	66.7	0.1	4.7	0.50
PCN-550	36.3	58.7	2.3	1.7	0.72
PCN-560	36.5	58.7	2.2	1.6	0.73
PCN-570	36.6	58.6	2.1	1.7	0.73
PCN-580	36.6	58.6	2.2	1.6	0.73
MCN-530	34.4	60.5	2.5	2.1	0.64
MCN-550	34.6	60.6	2.6	2.0	0.65
MCN-560	34.9	60.9	2.6	2.0	0.66
MCN-570	34.9	60.7	2.5	2.0	0.66
MCN-580	35.2	60.8	2.4	2.0	0.67
MCN-600	35.9	58.9	2.3	1.9	0.71

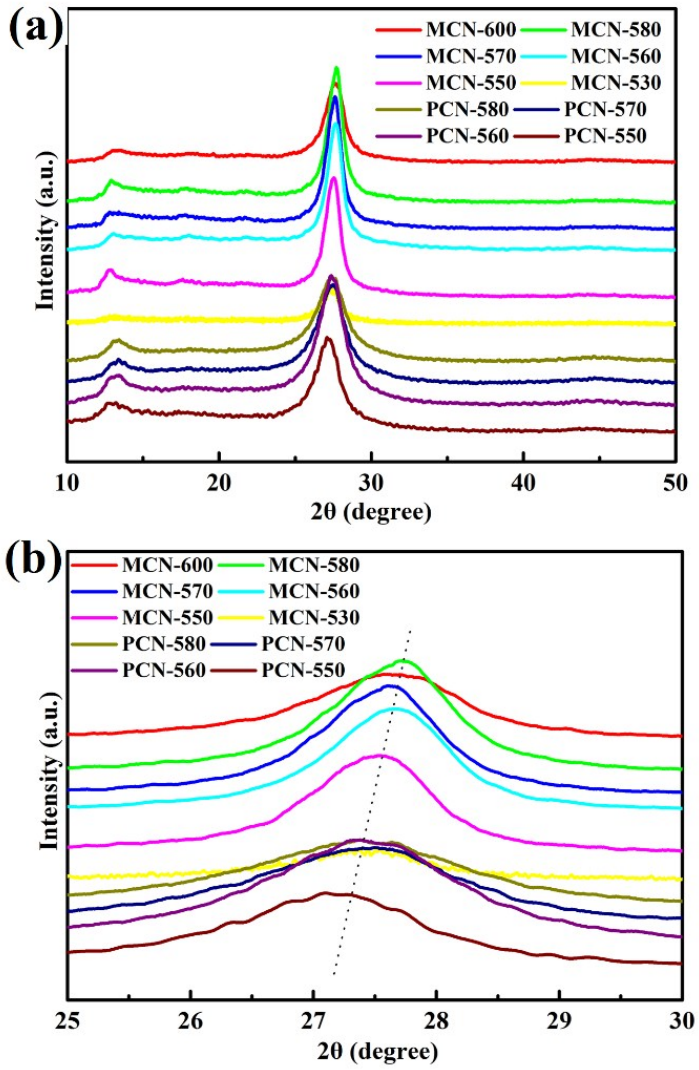

Figure S9 (a) XRD and (b) details of PCN and MCN materials in different sintering temperatures.

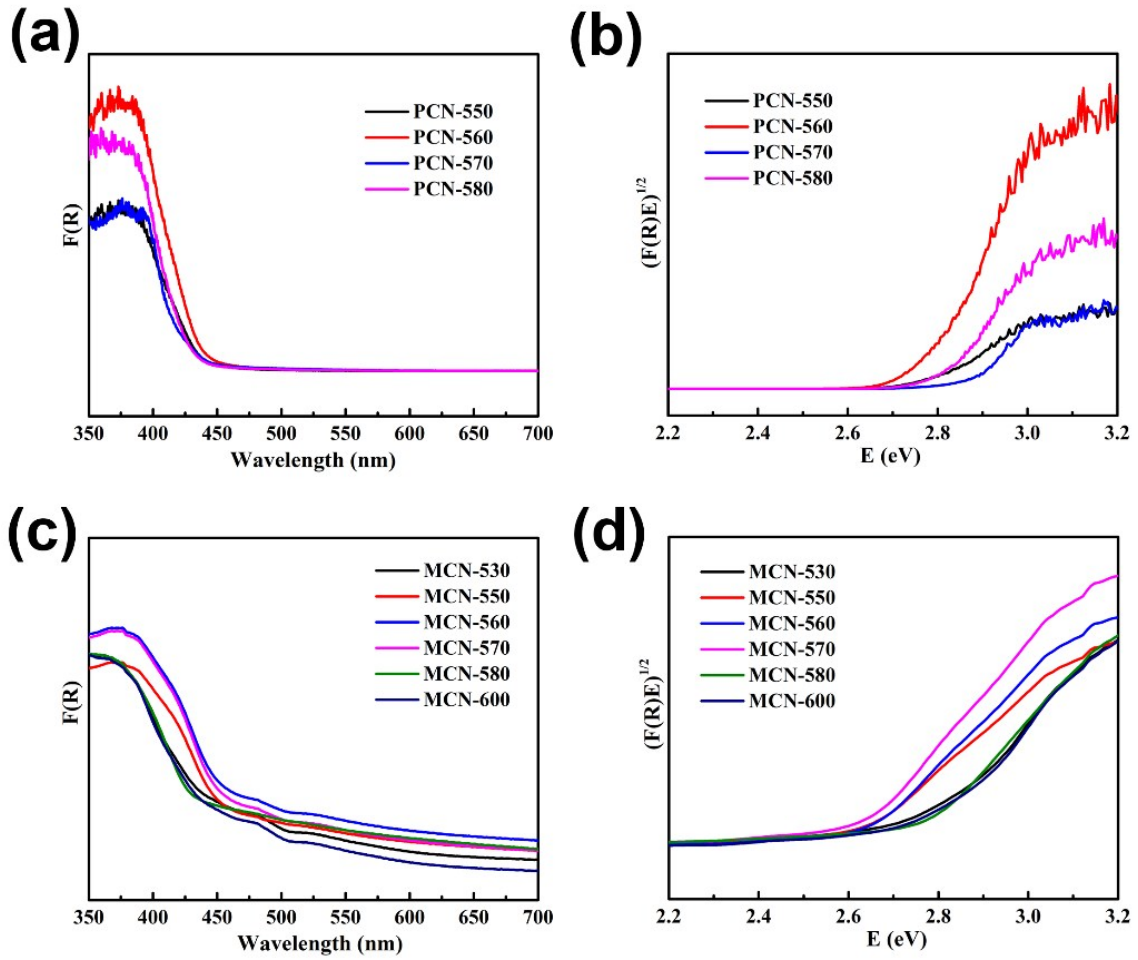

Figure S10 UV-vis absorption spectra and Plots of $(Ahv)^{1/2}$ vs photon energy (hν) for the band gap energy of (a, b) MCN materials and (c, d) PCN materials, respectively.

Table S4 Band gaps of PCN and MCN materials.

Material	Band Gap [eV]	Material	Band Gap [eV]
PCN-550	2.80	MCN-550	2.67
PCN-560	2.78	MCN-560	2.64
PCN-570	2.85	MCN-570	2.65
PCN-580	2.82	MCN-580	2.72
MCN-530	2.77	MCN-600	2.76

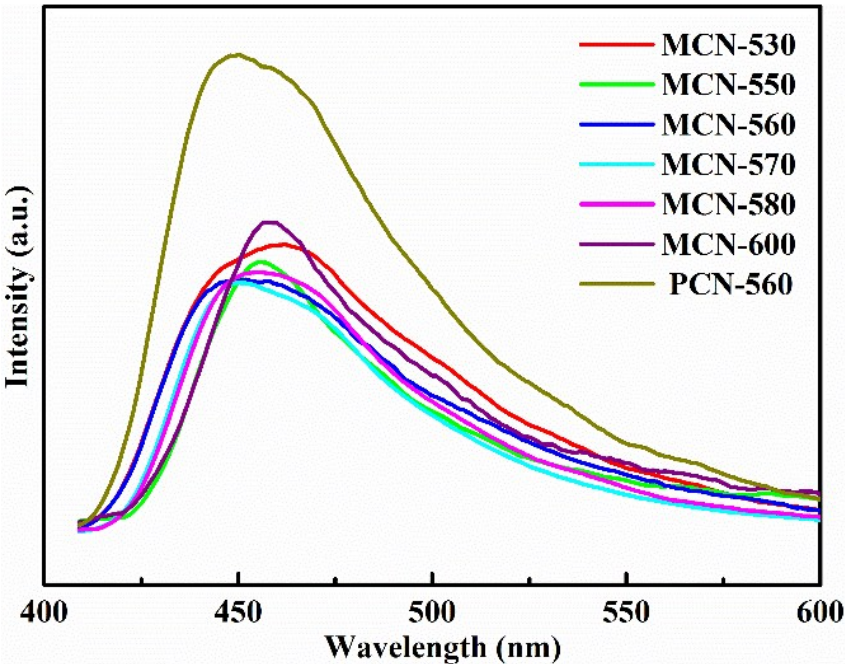

Figure S11 Photoluminescence spectra for MCN materials and PCN-560.

Table S5 Radiative Fluorescence Lifetimes and Their Relative Percentages of Photoexcited Charge Carriers in the PCN-560 and MCN-560.

Sample	Lifetime [ns]	Intensity [%]	Lifetime [ns]	Intensity [%]
MCN-560	0.83	28.32	5.95	71.68
PCN-560	0.90	35.13	5.71	64.87

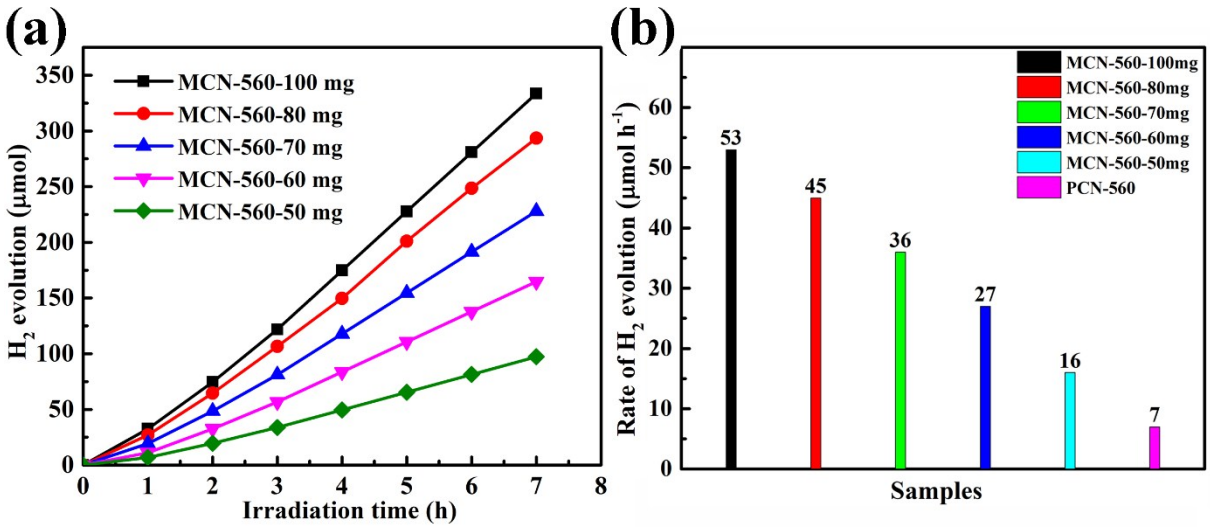

Figure S12 (a) yield and (b) rate of photo-catalytic H_2 evolution over different dosage of MCN-560 under visible light irradiation ($\lambda > 400$ nm).

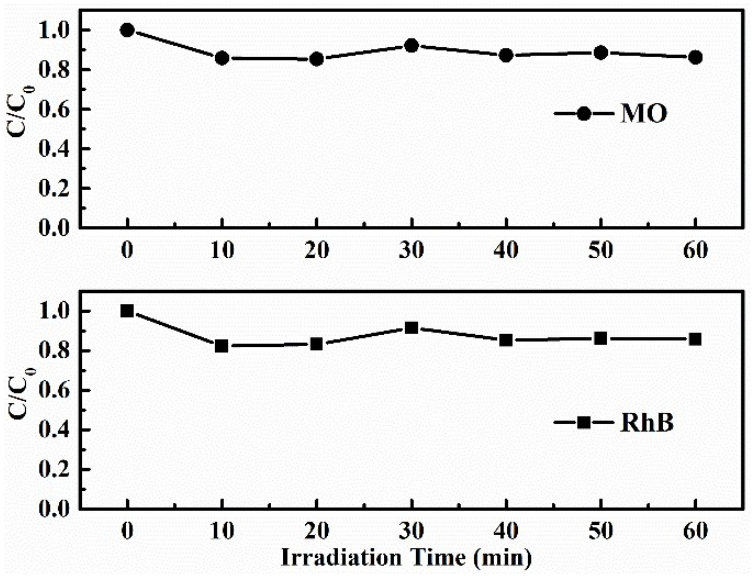

Figure S13 Dark absorption of RhB and MO over MCN-560.

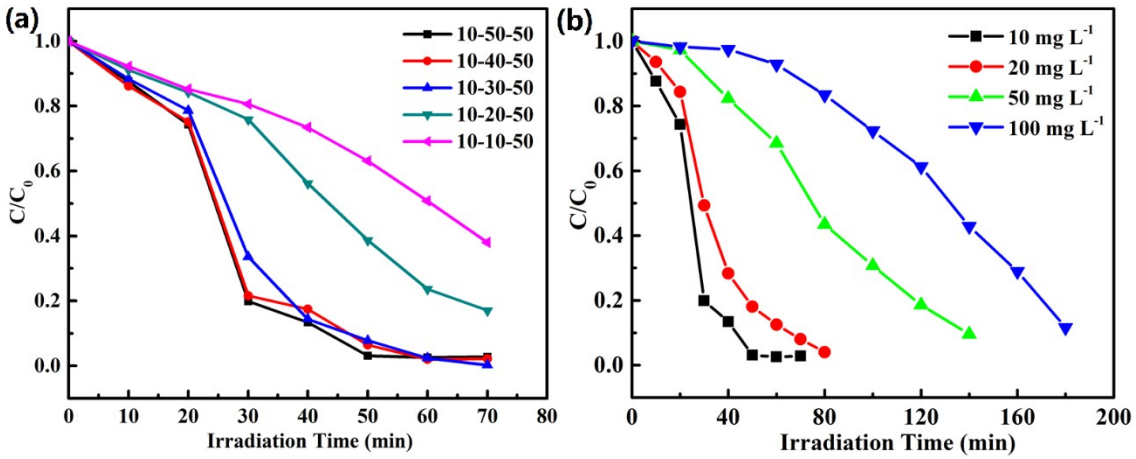

Figure S14 Photo-degradation of RhB over MCN-560 (a) in different dosages and (b) in different concentrations.

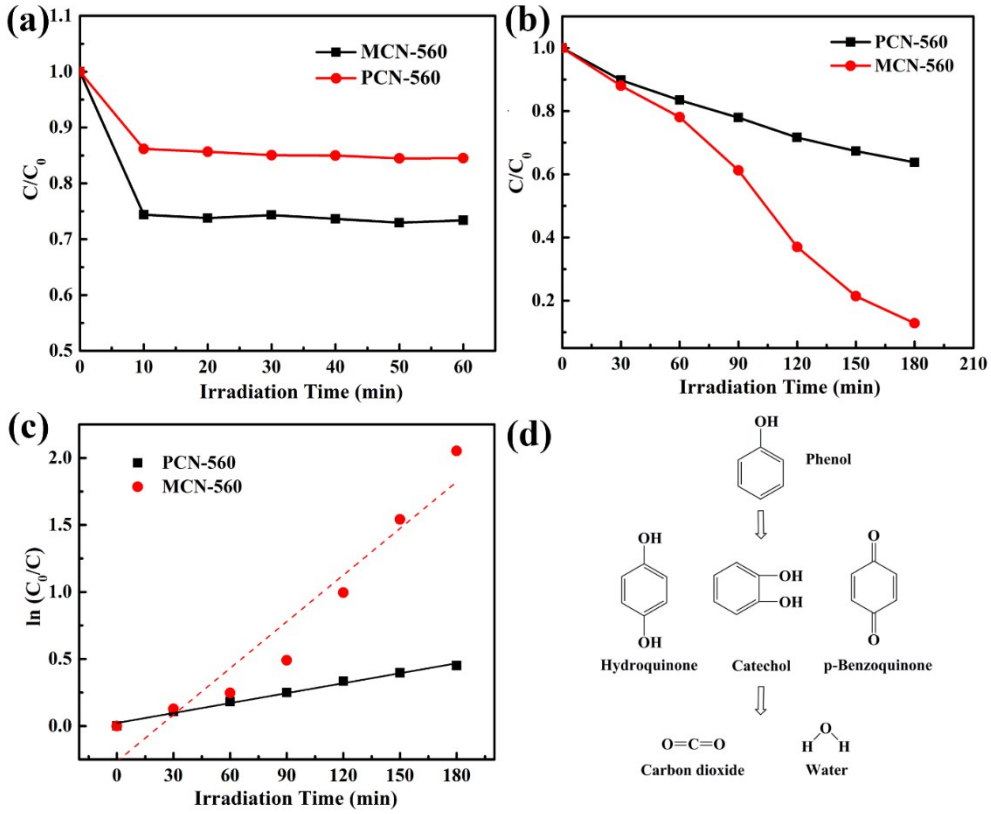

Figure S15 (a) Dark adsorption, (b) photo-catalysis, (c) kinetics and (d) possible mechanism of phenol degradation over PCN-560 and MCN-560 under visible light irradiation respectively.

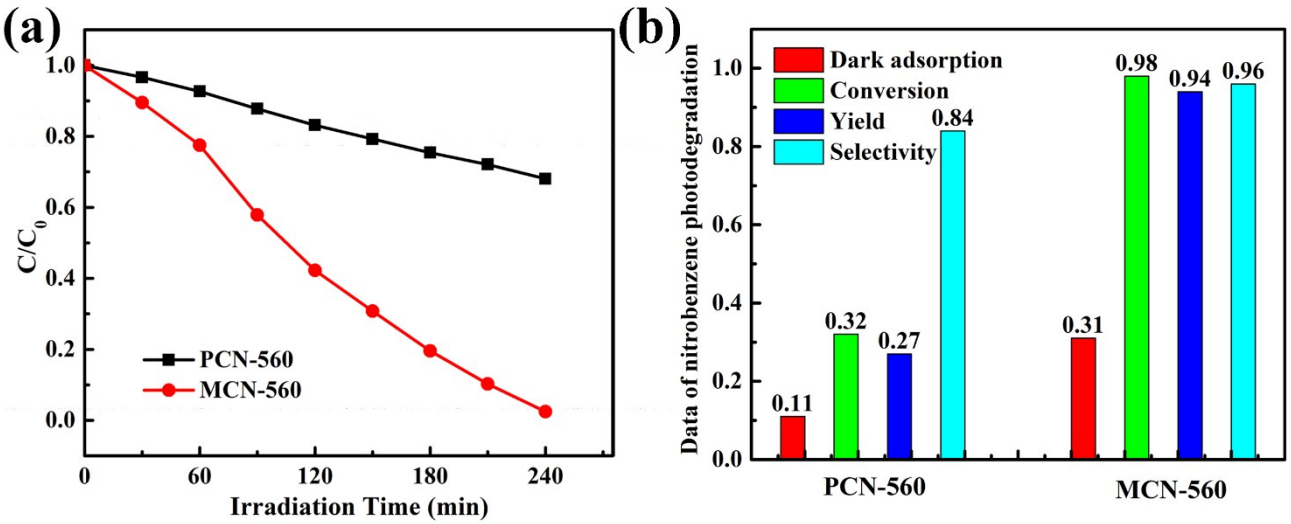

Figure S16 (a) Continuous photo-reduction of nitrobenzene and (b) dark adsorption, conversion, yield and selectivity of photo-reduction of nitrobenzene over PCN-560 and MCN-560 under visible light irradiation respectively.

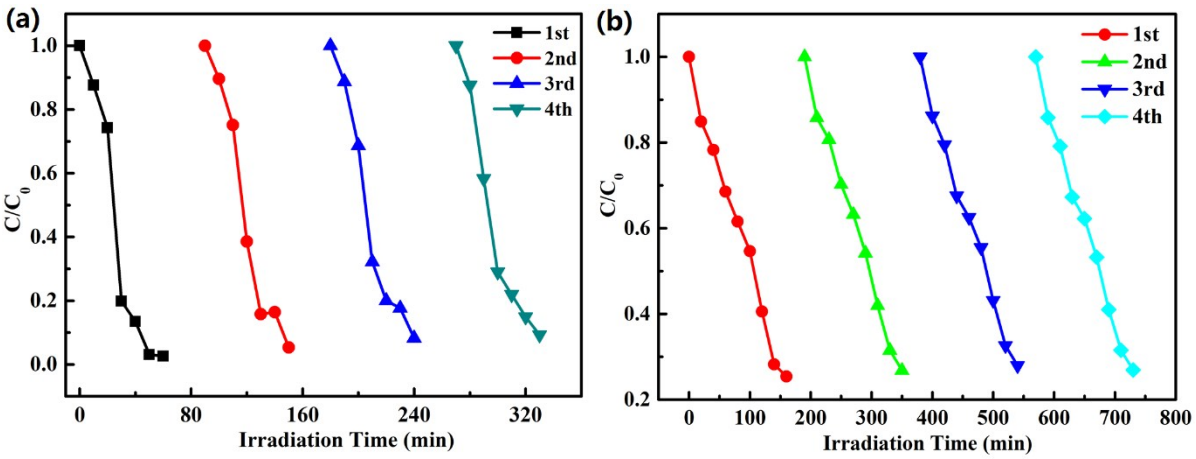

Figure S17 Cyclic test of (a) RhB and (b) MO degradation under visible light over MCN-560.

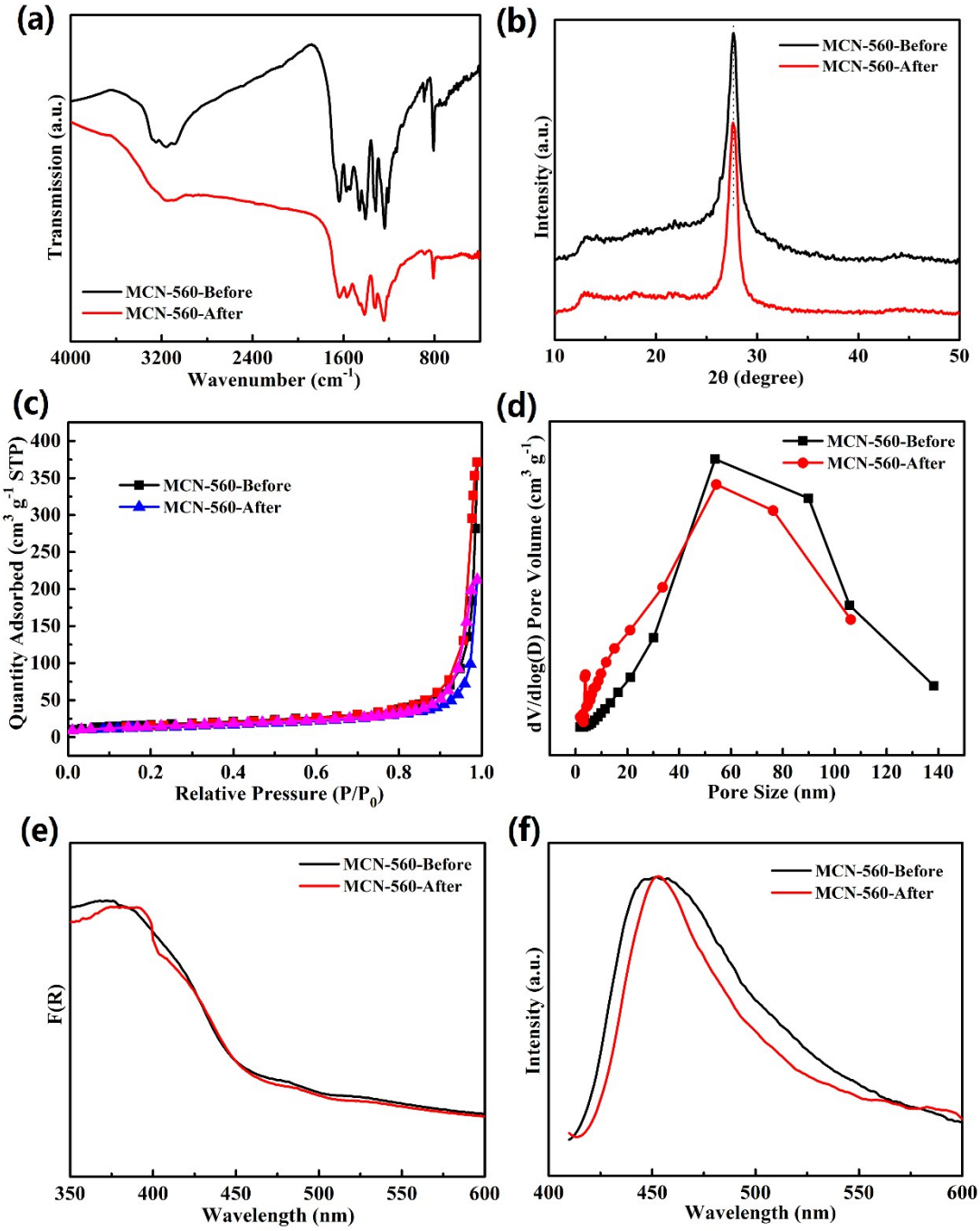

Figure S18 (a) FT-IR, (b) XRD, (c) nitrogen adsorption-desorption isotherms, (d) pore size distribution curves, (e) UV-Vis absorption spectra and (f) photoluminescence spectra of MCN-560 before and after photo-degradation.

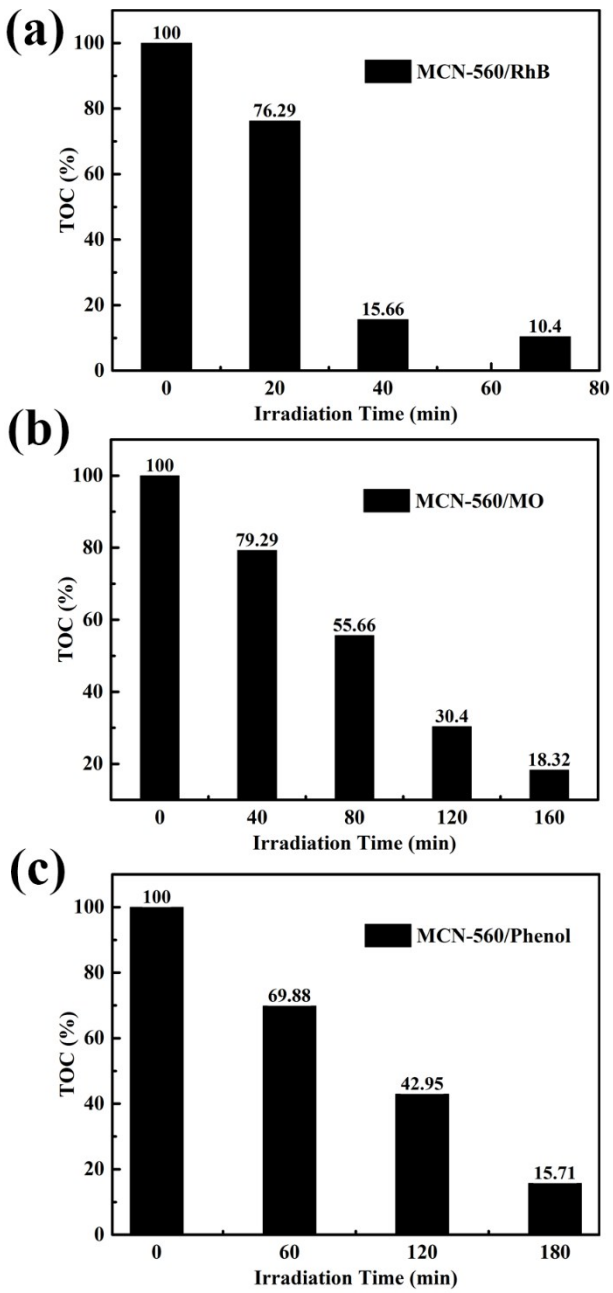

Figure S19 TOC removals as a function of light irradiation time for the solution of (a) RhB, (b) MO and (c) phenol in the MCN-560 photo-catalysis system.

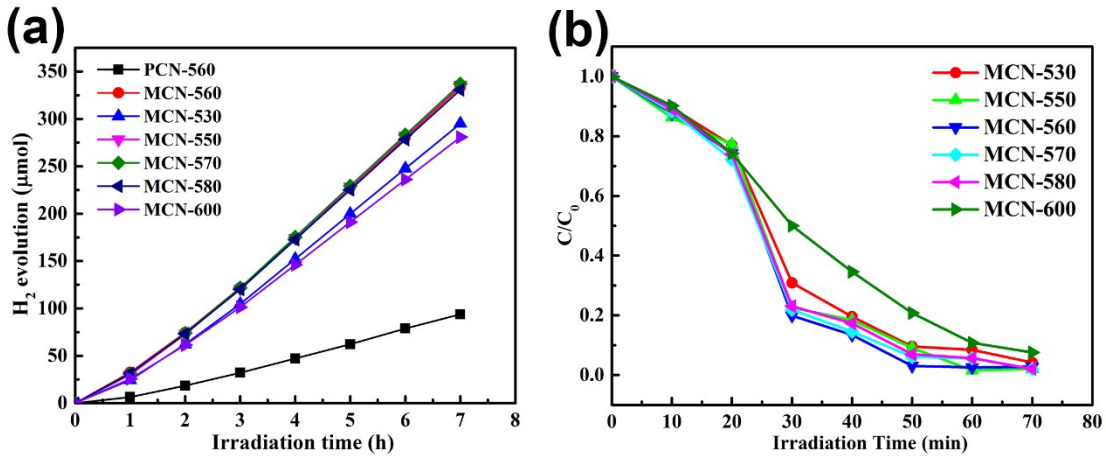

Figure S20 (a) H_2 evolution and (b) degradation of RhB over MCN-530, MCN-550, MCN-560, MCN-570, MCN-580, MCN-600 under visible light.

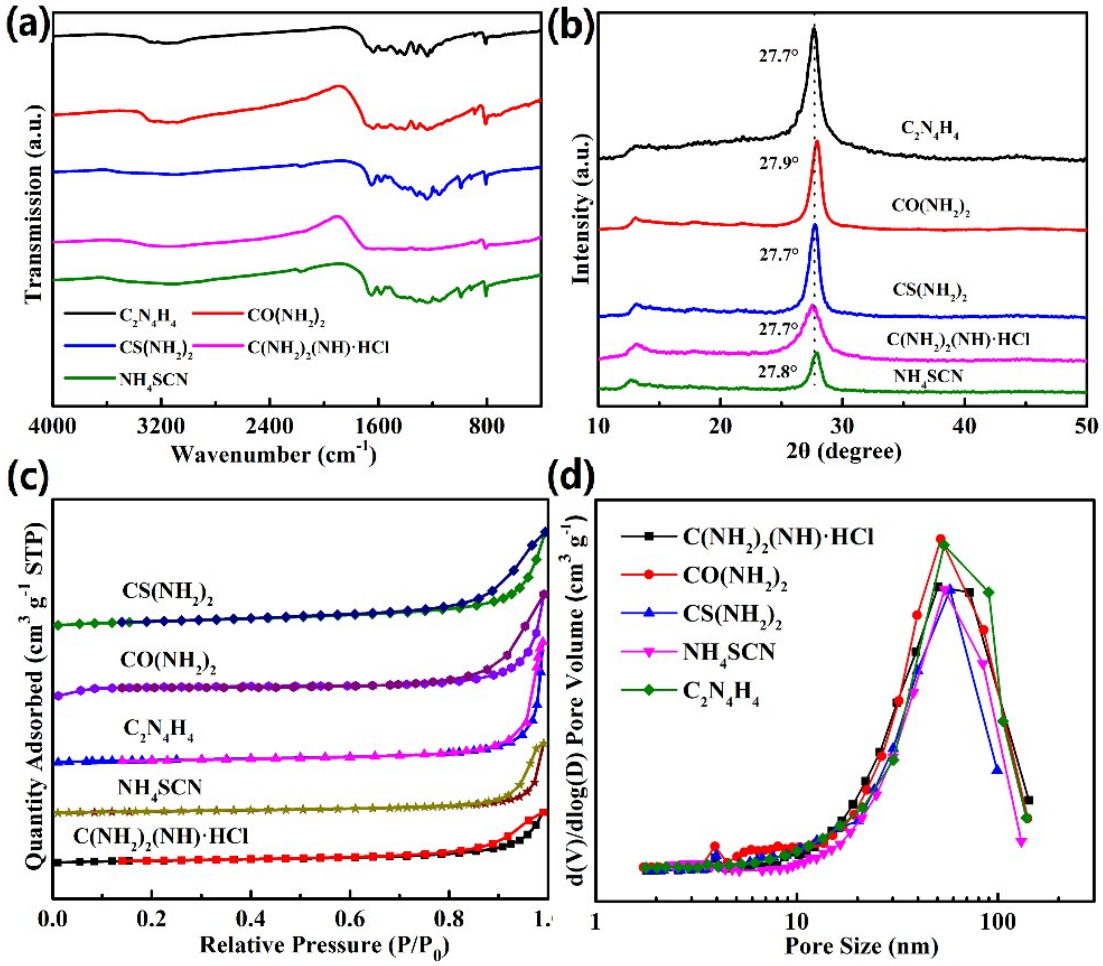

Figure S21 (a) FTIR, (b) XRD, (c) nitrogen adsorption-desorption isotherms and (d) the corresponding pore size distribution curves of MCN materials by different starting materials, Dicyandiamide ($C_2N_4H_4$), Urea ($CO(NH_2)_2$), Thiourea ($CS(NH_2)_2$), Ammonium thiocyanide (NH_4SCN) and Guanidine hydrochloride (CH_5N_3·HCl) under 560 °C.

Table S6 S_{BET} and pore volume of MCN materials by different starting materials.

Materials	S_{BET} [m^2 g^{-1}]	Pore Volume [cm^3 g^{-1}]
$C_2N_4H_4$ Dicyandiamide	58	0.15
$CO(NH_2)_2$ Urea	81	0.17
$CS(NH_2)_2$ Thiourea	72	0.16
$CH_5N_3 \cdot HCl$ Guanidine hydrochloride	63	0.15
NH_4SCN Ammonium thiocyanide	50	0.15

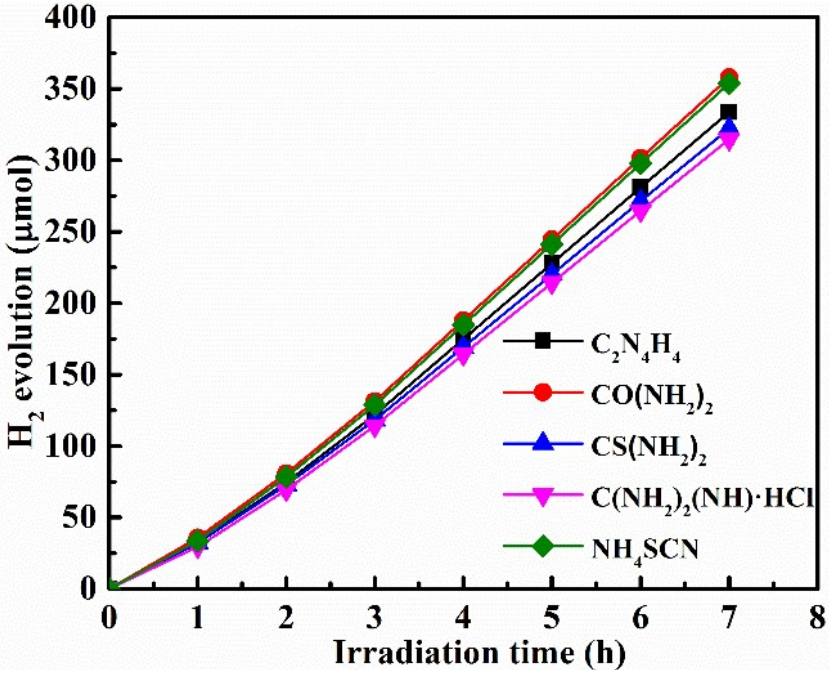

Figure S22 Photocatalytic H_2 evolution of MCN materials by different starting materials, Dicyandiamide ($C_2N_4H_4$), Urea ($CO(NH_2)_2$), Thiourea ($CS(NH_2)_2$), Ammonium thiocyanide (NH_4SCN) and Guanidine hydrochloride (CH_5N_3·HCl) under visible light irradiation.

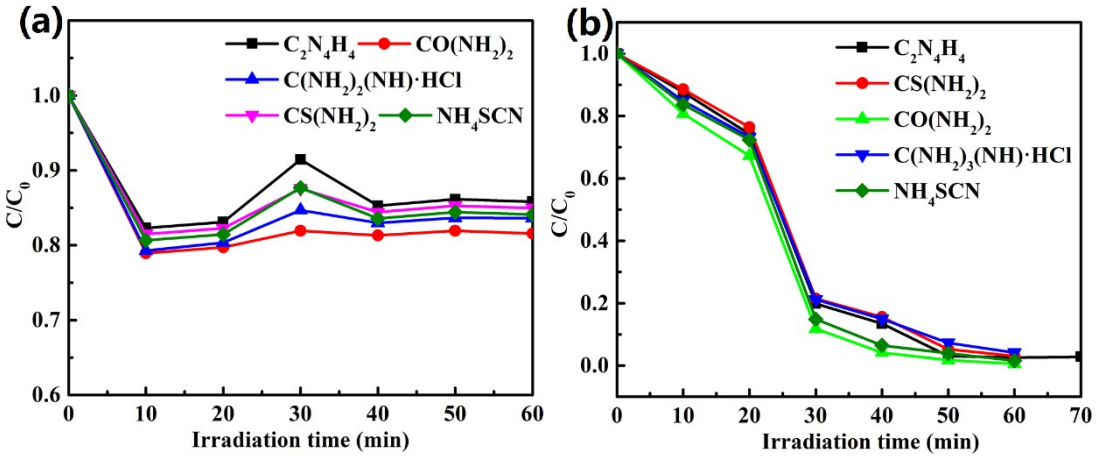

Figure S23 (a) Dark adsorption and (b) visible light irradiation degradation of MCN materials by different starting materials, Dicyandiamide ($C_2N_4H_4$), Urea ($CO(NH_2)_2$), Thiourea ($CS(NH_2)_2$), Ammonium thiocyanide (NH_4SCN) and Guanidine hydrochloride (CH_5N_3·HCl) under 560 °C.

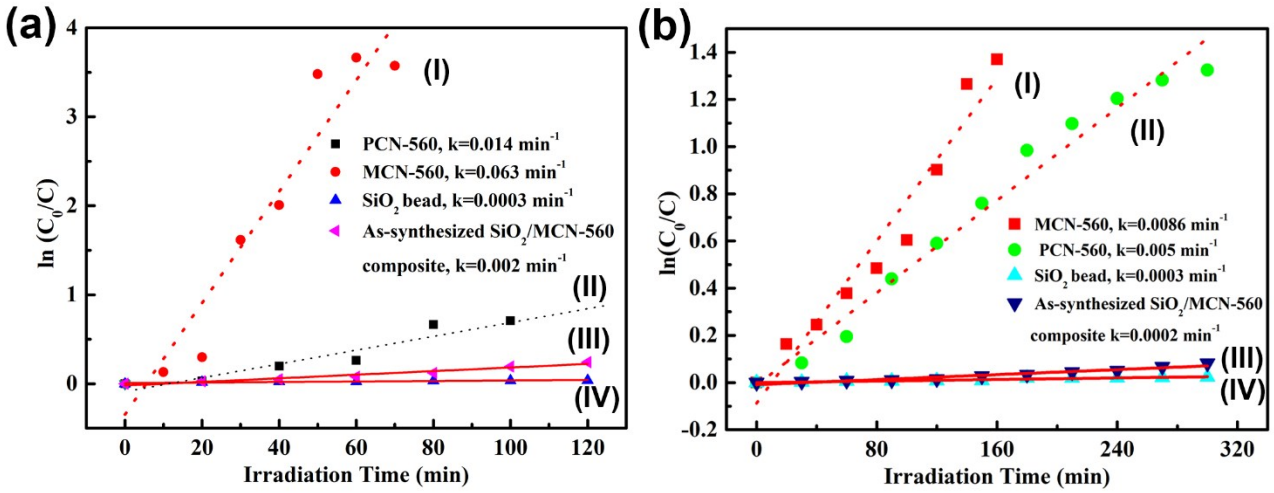

Figure S24 (a) Relationship between the dye RhB and (b) MO degradation efficiency and the light irradiation time for MCN-560 (I), PCN-560 (II), as synthesized SiO_2/MCN-560 (III) and SiO_2 beads (IV).

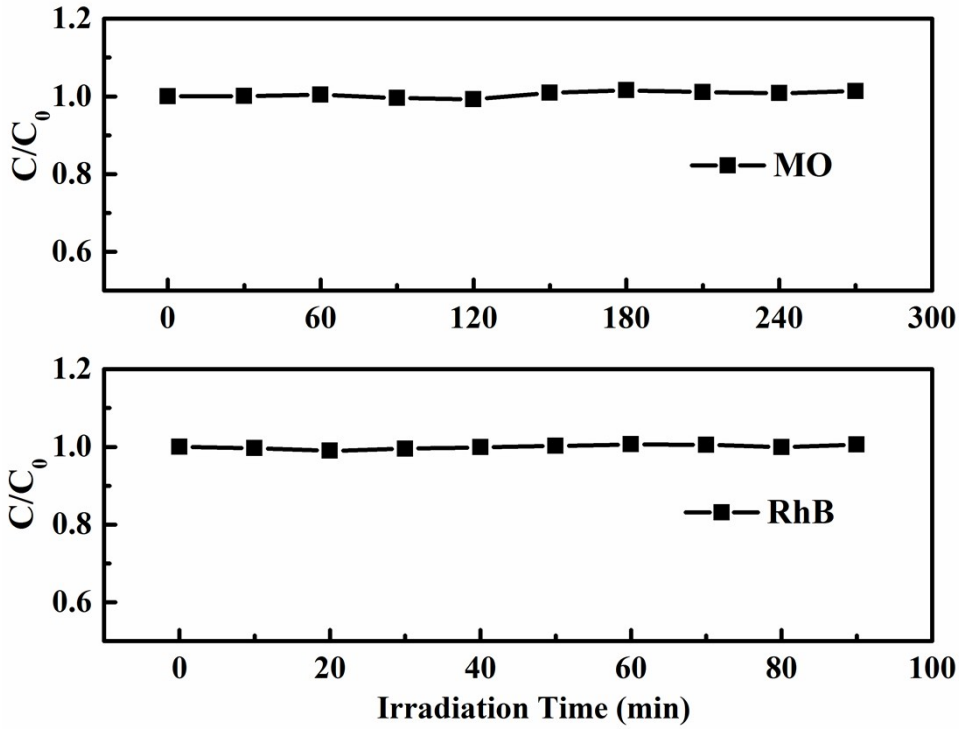

Figure S25 Photo-catalytic activities for self-degradation of RhB and MO degradation on MCN-560 under visible light irradiation.

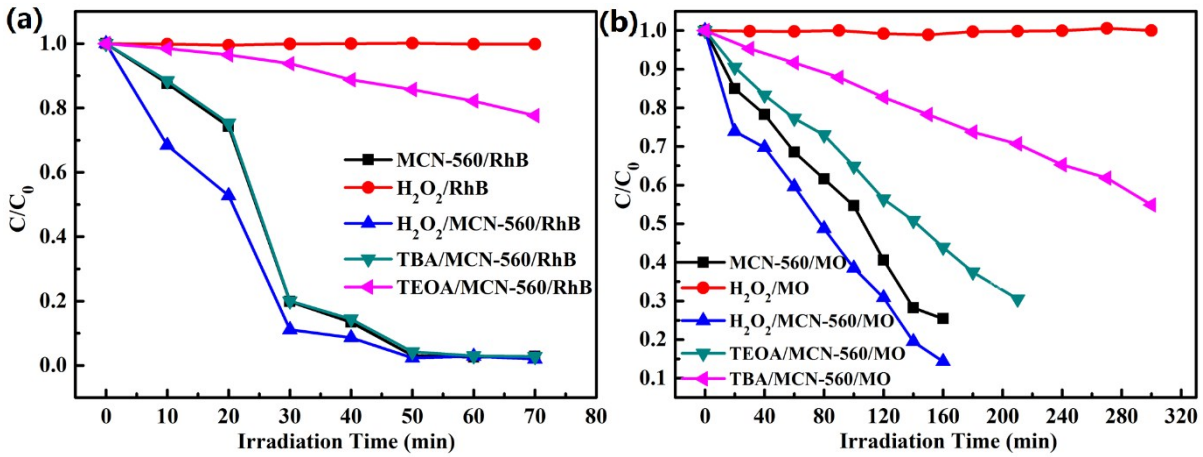

Figure S26 Comparison of photocatalytic activities for (a) RhB and (b) MO degradation in different photo-catalysis systems under visible light irradiation.